Precise 3D Indoor Localization Based on Wi-Fi FTM and Built-in Sensors□IEEE Internet of Things Journal

Article *in* IEEE Internet of Things Journal · June 2020

DOI: 10.1109/JIOT.2020.2999626

CITATIONS
0

READS
172

7 authors, including:

Yue Yu
Wuhan University
4 PUBLICATIONS **16** CITATIONS
SEE PROFILE

Ruizhi Chen
Texas A&M University - Corpus Christi
147 PUBLICATIONS **2,269** CITATIONS
SEE PROFILE

Liang Chen
Wuhan University
84 PUBLICATIONS **970** CITATIONS
SEE PROFILE

Shihao Xu
Wuhan University
2 PUBLICATIONS **8** CITATIONS
SEE PROFILE

Precise 3D Indoor Localization Based on Wi-Fi FTM and Built-in Sensors

Yue Yu, Ruizhi Chen*, Liang Chen, Shihao Xu, Wei Li, Yuan Wu and Haitao Zhou

***Abstract*—More and more applications of location-based services lead to the development of indoor positioning technology. As a part of the Internet of Things ecosystem, most existing indoor positioning algorithms are applied to specific situations, e.g., pedestrian navigation and target detection. To meet the high-precision indoor localization requirement, IEEE 802.11 included the Wi-Fi Fine Time Measurement protocol in 2016 which provides a novel approach for Wi-Fi ranging between the mobile terminal and Wi-Fi access point. This paper proposes a precise 3D indoor localization algorithm based on Wi-Fi Fine Time Measurement and smartphone built-in sensors (3D-WFBS). The adaptive extended Kalman filter is used to estimate the pedestrian's real-time heading and walking speed, and the received signal strength indication and round-trip time collected from Wi-Fi access points are combined for proximity detection and providing more accurate ranging results. In addition, the unscented particle filter is applied to fuse the results of adaptive extended Kalman filter, proximity detection and Wi-Fi ranging. Experimental results show that compared with the existing dead reckoning method and the other fusion methods, the proposed 3D-WFBS algorithm is proved to achieve meter-level indoor positioning accuracy in typical indoor scenes.**

***Index Terms*—Indoor localization, Wi-Fi Fine Time Measurement, built-in sensors, unscented particle filter**

I. INTRODUCTION

The Internet of Things (IoT) integrates sensing, communication, and computing technology. This will make the communication of human to human more convenient, and the communication of human to thing or thing to thing possible. As an important IoT based application, indoor positioning integrates sensing, communication, and artificial intelligence (AI) technology to provide a reliable location for the pedestrian. Relying on the accurate positioning service, route navigation in airports, shopping malls, and other indoor public areas can be easily achieved [1-2].

Global Navigation Satellite System (GNSS) is widely used for positioning outdoors which can provide meter-level localization accuracy. In GNSS-denied indoor environments, various indoor localization systems based on different techniques, such as ultra-wideband (UWB) [3], Bluetooth [4], Wi-Fi [5], EMG signal [6], and self-contained sensors [7] have been developed for location-based services (LBS).

At present, there are three main popular smartphone-based indoor localization methods: 1) Autonomous localization based on smartphone built-in sensors, usually using pedestrian dead reckoning (PDR) algorithm, by collecting the data from multiple sensors such as the accelerometer, magnetometer and gyroscope [8-9]; 2) The received signal strength indication (RSSI) based positioning, using RSSI signal to calculate the distance between mobile terminal (MT) and Bluetooth low energy (BLE) or Wi-Fi access point (AP) [10]. Besides, fingerprinting technique is also an effective approach to get the real-time location of pedestrians without knowing the position of local location stations in advance [11-12]; 3) Multi-source fusion based localization, There are always some limitations in the positioning principle or the distribution of single location source, thus, in order to achieve universal localization, the built-in sensors based method is usually combined with different location sources such as Wi-Fi or BLE to adapt to complex and changeable indoor environments [13-14].

IEEE 802.11-2016 standardized the Wi-Fi Fine Time Measurement (FTM) protocol which can provide meter-lever ranging accuracy according to the Wi-Fi alliance [15]. Ibrahim M and his partners analyzed the key factors and parameters which affect the Wi-Fi ranging performance based on the open platform and revisited standard error correction techniques for Wi-Fi FTM-based localization system [16]. Yu Y et al. [17] proposed a real-time Wi-Fi ranging model which reduce the impacts of clock deviation, non-line-of-sight (NLOS), and multipath, then used unscented Kalman Filter (UKF) to fuse data acquired from multiple sensors and Wi-Fi FTM and got the final positioning error within 2 m. Xu S H et al. [18] proposed an enhanced particle filter (PF) to fuse the multi-sensor data and Wi-Fi FTM data, using adaptive tilt compensation to improve the performance of heading estimation. The final localization accuracy is within 1 m in 86.7% of the dynamic cases when the number of particles is 2000.

Compared with RSSI, Wi-Fi FTM provides a more robust way for Wi-Fi ranging and can be used as a new location source with high accuracy. However, when giving a complex indoor environment which contains NLOS and multipath propagation, the distance error measured by Wi-Fi FTM cannot be easily eliminated due to the lack of line-of-sight (LOS) path. In

Manuscript received November XX, 2019; revised XX, XXXX; This work was supported by the National Key Research and Development Program of China under Grant 2016YFB0502200 and 2016YFB0502201 and the NSFC under Grant 91638203. (Corresponding author: Ruizhi Chen)

The authors are working together with the State Key Laboratory of Information Engineering in Surveying, Mapping and Remote Sensing (LIESMARS), Wuhan University, Wuhan 430000, China (e-mail: ruizhi.chen@whu.edu.cn).

addition, PDR-based positioning methods are affected by accuracy of step-length estimation and heading drift therefore cannot be used for a long time.

In order to solve these problems, this paper proposes a real-time 3D indoor localization algorithm based on Wi-Fi FTM and built-in sensors (3D-WFBS). The contributions of this work are summarized as follows:

1) This paper uses the adaptive extended Kalman filter (AEKF) to fuse tri-axial data acquired from the accelerometer, gyroscope and magnetometer and get the pedestrian's real-time speed and heading information with high precision.

2) This paper combines RSSI and round-trip time (RTT) signals acquired from local Wi-Fi APs to realize more accurate Wi-Fi ranging and proximity detection, the results of proximity detection are used to provide absolute altitude reference to barometer based altitude calculation.

3) Based on the results of AEKF, Wi-Fi ranging and proximity detection, 3D-WFBS is proposed. A real-time unscented particle filter (UPF) is applied to fuse the information acquired from Wi-Fi ranging and built-in sensors. The combination of two location sources effectively improves the final accuracy of 3D indoor localization.

This paper is organized as follows. Section II introduces the related work. Section III details the method of AEKF based heading and speed estimation. Section IV presents the 3D-WFBS algorithm. Section V describes the experimental results of proposed algorithm. Section VI concludes this paper.

II. Related Work

Various indoor positioning algorithms have been proposed in recent years, including inertial sensors, UWB, Wi-Fi, Bluetooth, and others. This section focuses on the Wi-Fi based positioning method and smartphone built-in sensors based positioning method.

A. Wi-Fi Based Indoor Positioning Method

Multiple characteristics estimated from Wi-Fi signals can be used for indoor localization such as received signal strength indication (RSSI), channel impulse response (CIR), time of arrival (TOA), angle of arrival (AOA), and channel state information (CSI).

D. Ciuonzo and Salvo Rossi used a wireless sensor network (WSN) to detect the position of the target with unknown emitted power and Gaussian noise. The Fusion Center is proposed to receive sensors decisions through error-prone Binary Symmetric Channels and provide a more-accurate global decision, the Locally-Optimum Detection framework is applied to reduce the computational complexity [19-20]. Arian Shoari and Alireza Seyedi also used binary Detectors for localization and developed Fisher information for estimation of target location and power [21].

Ferdews Tlili et al. [22] studied the time of localization in a WSN and used Multidimensional Scaling (MDS) method to get more accurate positioning result compared with the Trilateration method.

Saber Amri et al. [23] proposed a novel localization algorithm that used RSSI as an input of fuzzy inference system and calculated the distance between anchor and sensor nodes through channel flow. The experimental results proved its efficiency and energy-saving ability.

Safa Hamdoun et al. [24-25] considered different kinds of single /multiple antenna systems in the procedure of wireless transmission and got the meter-level performance of RSSI based positioning in case of using multiple antennas.

Xuyu Wang et al. [26] applied fingerprinting method in CSI based indoor localization, using Intel 5300 card to receive the CSI phase information and got the final localization accuracy within 2.23m in two typical experimental environments.

Wi-Fi FTM protocol is developed based on the time-of-arrival (TOA) and time-of-departure (TOD) methods which can also be used to measure the time of flight (TOF) [27-28]. Yuval Amizur et al. [29] introduced how the TOF works in details and a series of experiments were designed for localization estimation in a typical indoor environment. In order to reduce the negative impacts on unsynchronized time signal and multipath, AEKF was applied to fuse TOF measurements with IMU to enhance the performance of TOF system [30]. Nir Dvorecki et al. [31] proposed a "Siamese" artificial neural network (ANN) based on machine learning approach, which gives an effective solution to the influence of low bandwidth and go on to improve the ranging precision of Wi-Fi FTM. Niesen U et al. [32] proposed an improved dedicated short-range communication method by Wi-Fi FTM to perform outdoor inter-vehicle ranging. A timestamp compression method was discussed by discarding the most significant bits of each FTM frame.

Wi-Fi FTM is a point-to-point (P2P) single-user protocol, which includes an exchange of multiple message frames between an initiator such as mobile terminal and a responder such as Wi-Fi AP [33]. The whole procedure is described as follows. Firstly, the initiator sends a FTM request to responder, then the responder receives the request and returns an ACK signal, after that several FTM frameworks are exchanged between the responder and initiator. Fig.1 shows the whole procedure of protocol. The RTT information calculated by each FTM exchange is described in (1):

$$\mathrm{RTT}=\frac{(t_4-t_1)-(t_3-t_2)}{2} \tag{1}$$

where t_1 indicates the timestamp when the FTM structure first sent by the responder, t_2 represents the timestamp when the FTM structure received by the initiator, t_3 is the timestamp when the initiator returns the FTM structure to the responder and t_4 indicates the timestamp when the FTM structure finally received by the responder.

This article has been accepted for publication in a future issue of this journal, but has not been fully edited. Content may change prior to final publication. Citation information: DOI 10.1109/JIOT.2020.2999626, IEEE Internet of Things Journal

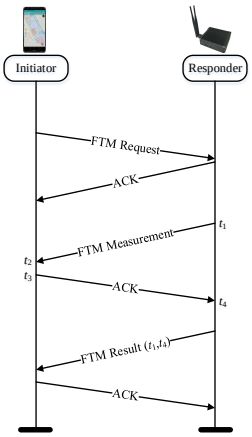

Fig. 1. Description of FTM Procedure

B. Built-in Sensors Based Indoor Positioning Method

PDR is based on smartphone built-in sensors to indicate the pedestrian's movement direction and location. Nowadays, most mobile terminals have integrated a wealth of micro-electromechanical-system (MEMS) based sensors which can be used for indoor localization purposes. The whole PDR structure can be divided into two steps: 1) step detection and step-length calculation; 2) heading fusion and correction.

Due to the mechanical nature of the human body, it is possible to define analytical expressions of the step detection and step-length calculation based on geometrical relations between some dimensions, angles, and displacements of different parts of the body [34]. The advantage of using biomechanical models is that it allows a good understanding of the relationships on which the estimation of the step length is built. However, due to the complexity of the human body and the great variability of people and scenarios, these models are usually simplifications and approximations that require calibration phases to adjust their performance to each specific user's walking pattern and walking pace [35-36].

Traditional Inertial Navigation Systems (INS) uses tri-axial gyroscopes to track orientation changes, while the output of integrated gyroscope in the intelligent terminal contains noise interference which would lead to the drift of pedestrian's real-time heading. The most widespread PDR constraint is provided by Zero Velocity Update (ZUPT). ZUPT was first used in a PDR context in the NavShoe project by Foxlin5, who reported good results in 2005 [37]. Magnetometers provide a direct estimate of the user's absolute heading, which is particularly useful for correcting the inevitable heading drift that occurs in the INS. Combining both gyroscope and magnetometer inputs has yielded some success since the two sensors have complementary error characteristics—gyroscopes give poor long-term orientation, while magnetometers are subject to short-term orientation errors. Xin Tong et al. [38] used a Double-step unscented Kalman filter (DUKF) to fuse the data acquired from accelerometer, gyroscope and magnetometer and get the RMSEs of fused attitude within 0.15◦. Valerie Renaudin et al. [39] proposed an attitude estimation algorithm based on a quaternion parameterization directly in the state vector and two opportunistic updates: magnetic angular rate update and acceleration gradient update, the final error of heading estimation was found to less than 7° after 1 km of walk.

C. Challenges of Smartphone Based Indoor Positioning

Wi-Fi FTM protocol is popular as IoT field is developing which provides a novel approach for TOF-based indoor localization. PDR is based on inertial devices, almost all the intelligent terminals contain MEMS sensors required by PDR. These two methods are the focus of recent research. However, summarizing the work of predecessors, this paper found that the TOF-based approach and PDR algorithm continue facing the following problems and challenges.

1) Differences in Pedestrian Characteristics. Pedestrian characteristics include for example heights, motion patterns and their step frequency. These would take into challenges in attitude calculation and step-length estimation. For example, the accuracy of step-length estimation can fluctuate ±40% with different height [40]. Besides, the way how people use smartphones can also influence the method of heading fusion, such as handheld, calling near the ear, swaying in the hand, and putting in the pant pocket. In order to improve the accuracy of localization, these different modes of smartphones should be recognized and classified [41].

2) Cumulative Error of Inertial Sensors: In PDR, the current location is based on the continuous reckoning of the previous location and pedestrian steps. The step-length error and heading deviation caused by cumulative error of inertial sensors will influence positioning accuracy. Fang et al. [42] tested the step length estimator proposed in [40] on a 1.2 km course in indoor and outdoor environment on different terrains and got the overall distance estimation error with personal calibration was about ±3% and ±8% without calibration across the variety of subjects. Combettes C et al. [43] proposed a novel walking direction estimation algorithm based on statistical models and likelihood maximization which can adjust to different people and their activities. A 1.4° to 15.3° error on the walking direction estimates is found over several "1km walk" tests indoors.

3) Indoor Environment Differences: Different building materials and indoor structures form different indoor environments. In different indoor environments, the propagation path and the loss in the propagation process are different, which lead to different signal propagation models especially when using RSSI based localization methods [44]. Compared with RSSI, TOF based methods are less influenced by multipath propagation, but is affected by NLOS. When giving a complex indoor scenario where the direct transmission path between the transceivers is blocked, the distance errors measured by TOF methods cannot be easily eliminated due to its measurement mechanism [45-46].

It can be found from previous studies that the characteristics extracted from Wi-Fi signals such as RSSI, CSI, and TOF are normally subjected to complex indoor environments due to the NLOS and multipath effects and Wi-Fi FTM proves better ranging accuracy compared with other acquired Wi-Fi characteristics in NLOS and multipath contained environments,

This article has been accepted for publication in a future issue of this journal, but has not been fully edited. Content may change prior to final publication. Citation information: DOI 10.1109/JIOT.2020.2999626, IEEE Internet of Things Journal

which can be used as a new indoor location source. Built-in sensors based localization method performs accurate location results in short time period but cannot be used for a long time. Thus, these two different location sources should be combined in order to get higher localization accuracy.

To improve the accuracy and flexibility of the indoor positioning, this paper proposes the 3D-WFBS algorithm. Based on previous studies, this paper provides a concrete solution with considering the above challenges. The 3D-WFBS combines Wi-Fi FTM and PDR to make the two advantages complementary. Firstly, the calibrated magnetometer data and compensated accelerometer and gyroscope data are fused by AEKF to get the real-time walking speed and heading information, and the barometer data is used to provide the deviation of the altitude information; Secondly, the RSSI and RTT data acquired from surrounding Wi-Fi APs are used for ranging fusion and proximity detection and detected Wi-Fi AP based landmarks are used to provide the absolute altitude information which can be used to calibrate the barometer based altitude calculation; Finally, a real-time UPF is applied to fuse the walking speed, heading, altitude and fused Wi-Fi ranging information and then the meter-level 3D localization performance can be achieved. The whole framework of proposed 3D-WFBS is shown in Fig.2.

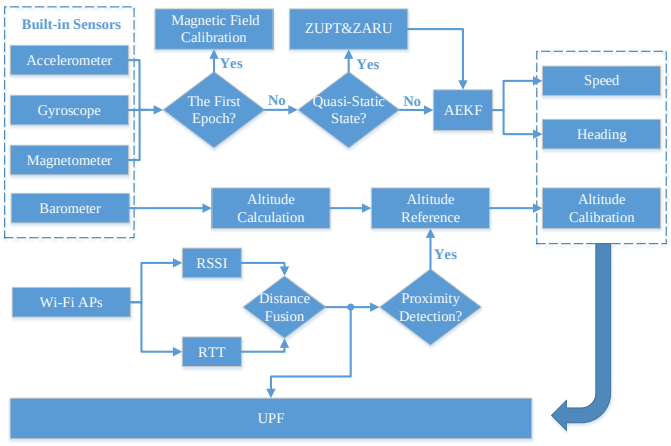

Fig. 2. Framework of 3D-WFBS algorithm

III. Heading and Walking Speed Estimation

The estimation of pedestrian's heading and walking speed comprises the main part of PDR based positioning method. The accuracy of indoor localization is affected by cumulative error originated from inertial sensors, external linear acceleration and magnetic field interference. In this section, AEKF is applied to fuse the pre-processed data collected from built-in sensors to overcome the cumulative error and environmental disturbance.

A. Step Detection and Walking Speed Measurement

According to the physiological characteristics of pedestrians' walking pattern, the output waveform of accelerometer's tri-axial modulus changes periodically during walking periods, so the periodicity and characteristic value can be used to detect gait [47]. The modulus of tri-axial acceleration data is defined in (2):

$$\text{Acc\_Norm} = \sqrt{a_x^{\,2} + a_y^{\,2} + a_z^{\,2}} \tag{2}$$

where Acc_Norm indicates the modules of tri-axial acceleration data, a_x, a_y, and a_z represent the x, y, and z axis data acquired from the accelerometer.

The output waveform of the original acceleration modulus contains noise, which would lead to erroneous steps and is not conducive to step detection. After filtering the original data by digital low-pass filter, more obvious single peak curves can be obtained.

Pedestrians may produce small jitters when walking with mobile terminals, the output waveform of the accelerometer modulus would also appear multiple peak values, thus, it is necessary to set thresholds to eliminate the step-counting error caused by jitters. The step detection algorithm adopts threshold method and sets threshold conditions which are shown in (3):

$$\begin{cases} \Delta T > T_{Th} \\ \left|\text{Acc\_norm} - g\right| < A_{Th} \end{cases} \tag{3}$$

where ΔT indicates the time interval between two adjacent step cycles, g represents the local gravity acceleration, and the time and peak thresholds are set as T_{Th} and A_{Th} respectively. The performance of final step detection is shown in Fig.3.

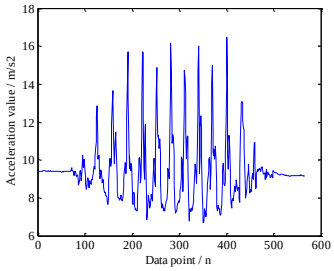

Fig. 3(a). Before Processed

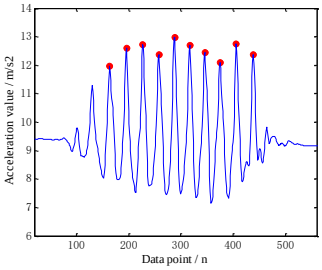

Fig. 3(b) After Processed

Two different kinds of step-length estimation models are used in this paper to calculate the walking speed. The empirical model between the modulus and step size of commonly used accelerometers is shown below [48]:

$$L_{\text{step}}^{1} = K\sqrt[4]{A_{\max} - A_{\min}} \tag{4}$$

where $A_{\max}$ and $A_{\min}$ represent the maximum and minimum values of the norm of acceleration during one step period, K indicates the ratio of the estimated distance and the ground-truth distance which is shown below:

$$K = \frac{d_{\text{estimated}}}{d_{\text{true}}} \tag{5}$$

It is found in [49] that the pedestrian's height and step frequency can also affect the accuracy of step-length estimation, in this paper, a linear model including pedestrian height and step frequency is also used:

$$L_{\text{step}}^{2} = [0.7 + a(H - 1.75) + b\frac{(SF - 1.79)H}{1.75}]c \tag{6}$$

where L_{step}^{2} and SF represent the step length and step frequency, respectively, H is the height of the pedestrian which is manually inserted in this step model, and a, b, and c are model parameters.

Because the pedestrian's height, attitude and walking

This article has been accepted for publication in a future issue of this journal, but has not been fully edited. Content may change prior to final publication. Citation information: DOI 10.1109/JIOT.2020.2999626, IEEE Internet of Things Journal

frequency are different, users must train the model before using in order to obtain the optimal model parameters. However, this method is extremely inconvenient for users to use, so it is necessary to design an adaptive algorithm to automatically adjust the calibration parameter in order to meet the needs of users.

Taking pedestrians' height, step frequency and acceleration variation into consideration, two different kinds of walking speeds are calculated as follow:

$$\boldsymbol{V}^i(k) = \boldsymbol{V}^i(k-1) + SF \cdot \Delta L^i_{\text{step}}(k), i = 1, 2 \tag{7}$$

where *SF* represents the step frequency, $\Delta L^i_{\text{step}}(k)$ indicates the change of step-length, $\boldsymbol{V}^i(k)$ represents real-time walking speed, the above two kinds of walking speed are fused by AEKF to get the optimized speed estimation result.

B. Adaptive Heading and Speed Fusion

According to the discrete time model of attitude updating by gyroscope quaternion method and the velocity parameter calculated by step-length model in (4), the state equation of AEKF can be obtained using rotating quaternion and velocity as the state vector:

$$\boldsymbol{x}_k = \begin{bmatrix} \boldsymbol{Q}_k \\ \boldsymbol{V}_k \end{bmatrix} = \begin{bmatrix} F_{k,k-1}(\boldsymbol{\omega}_k, T_s) & 0 \\ 0 & 1 \end{bmatrix} \boldsymbol{x}_{k-1} + \begin{bmatrix} 0 \\ \Delta \boldsymbol{V}^1 \end{bmatrix} + \boldsymbol{w}_k \tag{8}$$

where $\boldsymbol{x}_k$ contains current moment's quaternion $\boldsymbol{Q}_k$ and walking speed $\boldsymbol{V}_k$ calculated by (7) in case of $i = 1$, $\Delta \boldsymbol{V}^1_{\text{speed}} = SF \cdot \Delta L^1_{\text{step}}(k)$ represents the velocity variation, $\boldsymbol{F}_{k,k-1}(\boldsymbol{\omega}_k, T_s)$ represents the state transition matrix which is used for quaternion updating, $\boldsymbol{\omega}_k$ indicates the angular velocity of gyroscope, T_s indicates the sampling rate, $\boldsymbol{w}_k = [\boldsymbol{w}_k^q \quad w_k^v]^{\mathrm{T}}$ represents the state noise with a state covariance matrix $\boldsymbol{U}_k$.

The sensor data acquired from the accelerometer and magnetometer can also be used to calculate pedestrian's real-time attitude information, the measured values of the normalized tri-axial acceleration, the normalized tri-axial magnetic value and walking speed calculated by (7) in case of $i = 2$ are taken as the observed vector, the observation equation is shown in (9):

$$\boldsymbol{z}_k = h(\boldsymbol{x}_k) + \boldsymbol{v}_k = \begin{bmatrix} \boldsymbol{T}_n^b(\boldsymbol{Q}_k) & 0 & 0 \\ 0 & \boldsymbol{T}_n^b(\boldsymbol{Q}_k) & 0 \\ 0 & 0 & 1 \end{bmatrix} \begin{bmatrix} \boldsymbol{g} \\ \boldsymbol{m} \\ \boldsymbol{V}_k \end{bmatrix} + \begin{bmatrix} \boldsymbol{v}_k^a \\ \boldsymbol{v}_k^m \\ v_k^s \end{bmatrix} \tag{9}$$

In which:

$$\boldsymbol{T}_n^b = \begin{bmatrix} 1-2(q_2^2+q_3^2) & 2(q_1 q_2 + q_0 q_3) & 2(q_1 q_3 - q_0 q_2) \\ 2(q_1 q_2 - q_0 q_3) & 1-2(q_1^2+q_3^2) & 2(q_2 q_3 + q_0 q_1) \\ 2(q_1 q_3 + q_0 q_2) & 2(q_2 q_3 - q_0 q_1) & 1-(q_1^2+q_2^2) \end{bmatrix} \tag{10}$$

$$\boldsymbol{g} = \begin{bmatrix} 0 & 0 & 1 \end{bmatrix} \tag{11}$$

$$\boldsymbol{m} = \begin{bmatrix} 0 & b_y & b_z \end{bmatrix} \tag{12}$$

The observed noise matrix can be expressed as:

$$\boldsymbol{R} = \begin{bmatrix} \sigma_a^2 \boldsymbol{I} & 0 & 0 \\ 0 & \sigma_m^2 \boldsymbol{I} & 0 \\ 0 & 0 & \sigma_v^2 \end{bmatrix} \tag{13}$$

Because the relationship between the state vector and the measurement vector of the observation equation is non-linear, it is necessary to linearize the $h(\boldsymbol{x}_k)$ in (9), and the measured matrix is linearized by (14). The observation Jacobian matrix obtained is shown in (15):

$$\boldsymbol{H} = \frac{\partial h(\boldsymbol{x}_k)}{\partial \boldsymbol{x}_k}\Big|_{\boldsymbol{x}_k = \bar{\boldsymbol{x}_k}} \tag{14}$$

$$\boldsymbol{H} = \begin{bmatrix} -2q_2 & 2q_3 & -2q_0 & 2q_1 & 0 \\ 2q_1 & 2q_0 & 2q_3 & 2q_2 & 0 \\ 4q_0 & 0 & 0 & 4q_3 & 0 \\ 2b_y q_3 - 2b_z q_2 & 2b_y q_2 + 2b_z q_3 & 2b_y q_1 - 2b_z q_0 & 2b_y q_0 + 2b_z q_1 & 0 \\ 4b_y q_0 + 2b_z q_1 & 2b_z q_0 & 4b_y q_2 + 2b_z q_3 & 2b_z q_2 & 0 \\ -2b_y q_1 + 4b_z q_0 & -2b_y q_0 & 2b_y q_3 & 2b_y q_2 + 4b_z q_3 & 0 \\ 0 & 0 & 0 & 0 & 1 \end{bmatrix} \tag{15}$$

The measurement noise of accelerometer and magnetometer basically remain unchanged in the static and non-magnetic cases, but when the mobile terminal produces large linear acceleration or magnetic interference exists in the surrounding environment, the actual measurement values of accelerometer and magnetometer contains uncertainty error. To solve the problem, this paper constructs the adaptive observation variance σ_a^2, σ_m^2 and σ_v^2 to adjust the weights of measured values, which can be used in dynamic acceleration and magnetic interference contained environments.

$$\sigma_a^2 = k_{a1}(\|\boldsymbol{a}_k\| - \|\mathbf{g}\|) + k_{a2} var(\|\boldsymbol{a}_{k\text{-}N}\| : \|\boldsymbol{a}_k\|) \tag{16}$$

$$\sigma_m^2 = k_{m_1} var(\|\theta_{k\text{-}N}\| : \|\theta_k\|) + k_{m_2} var(\|\boldsymbol{m}_{k\text{-}N}\| : \|\boldsymbol{m}_k\|) \tag{17}$$

$$\sigma_v^2 = k_v var(\|\boldsymbol{V}^1 - \boldsymbol{V}^2\|_{k\text{-}N:k}) \tag{18}$$

In (16), the deviation between acceleration modulus and standard gravity value and the variance of acceleration modulus are used as eigenvalues to adjust the weight of acceleration data in AEKF. In (17), the variance of heading calculated by magnetometer and modulus of magnetometer data are used to detect the quasi-static magnetic field (QSMF) in surrounding environments [50], the magnetometer data in QSMF periods can be used after calibration, and the absolute heading reference provided by magnetometer data will be used to correct cumulative error caused by gyroscope. In (18), the deviation between two kinds of speed is used to adjust the weight of observed value.

When the mobile terminal carried by pedestrian produces large linear acceleration or is disturbed by external magnetic field, the weights of accelerometer and magnetometer in AEKF will decline, which leads to the increasing weight of the gyroscope calculation, thus, the influence of linear acceleration and external magnetic interference will be reduced. The whole AEKF procedure is shown in Table I:

This article has been accepted for publication in a future issue of this journal, but has not been fully edited. Content may change prior to final publication. Citation information: DOI 10.1109/JIOT.2020.2999626, IEEE Internet of Things Journal

TABLE I
THE PROCEDURE OF EKF FUSION

Algorithm: The EKF based Heading and Speed Estimation

1) State vector prediction:

$$\boldsymbol{x}_k^- = \boldsymbol{F}_{k,k-1}\boldsymbol{x}_{k-1} \tag{19}$$

2) Covariance matrix prediction:

$$\boldsymbol{P}_k^- = \boldsymbol{F}_{k,k-1}\boldsymbol{P}_{k-1}\boldsymbol{F}_{k,k-1}{}^{\mathrm{T}} + \boldsymbol{U}_k \tag{20}$$

3) Observation Matrix linearization:

$$\boldsymbol{H} = \frac{\partial h(\boldsymbol{x}_k)}{\partial \boldsymbol{x}_k}\Big|_{\boldsymbol{x}_k = \boldsymbol{x}_k^-} \tag{21}$$

4) Kalman gain calculation:

$$\boldsymbol{K}_k(k) = \boldsymbol{P}_k^-\boldsymbol{H}_k{}^{\mathrm{T}}\left[\boldsymbol{H}_k\boldsymbol{P}_k^-\boldsymbol{H}_k{}^{\mathrm{T}} + \boldsymbol{R}_k\right]^{-1} \tag{22}$$

5) State vector update:

$$\boldsymbol{x}_k = \boldsymbol{x}_k^- + \boldsymbol{K}_k\left[\boldsymbol{z}_k - \boldsymbol{H}_k\boldsymbol{x}_k^-\right] \tag{23}$$

6) Covariance matrix update.

$$\boldsymbol{P}_k = \boldsymbol{P}_k^- - \boldsymbol{K}_k\boldsymbol{H}_k\boldsymbol{P}_k^- \tag{24}$$

IV. INTEGRATED LOCALIZATION BASED ON UPF

This work uses Wi-Fi ranging and built-in sensors to estimate the pedestrian's position. To realize a more robust Wi-Fi ranging, RSSI and FTM information are combined in this section, and the UPF is applied to fuse all the location sources together to achieve real-time 3D indoor localization.

A. Ranging Fusion and Proximity Detection Based on Wi-Fi FTM and RSSI

Wi-Fi FTM can provide accurate ranging performance in case of LOS, but is affected by random and NLOS errors because of its measurement mechanism [15], the observed distance of Wi-Fi FTM is usually described as follows:

$$L_{\text{observed}} = L_{\text{FTM}} + d_N + d_{\text{random}} \tag{25}$$

where L_{observed} represents observed value which contains the NLOS error d_N and random error d_{random}, L_{FTM} indicates the ground truth value of Wi-Fi FTM. In addition, the ranging performance of Wi-Fi FTM in short distance is relatively poor because the variance of the ranging error indoors sometimes can reach 1 m or more [16].

The RSSI signal acquired from Wi-Fi AP suffers from multipath propagation in typical indoor environments, besides, RSSI ranging accuracy would decline significantly when distance between smartphone and Wi-Fi AP increases [51]. Thus, the RSSI value acquired from the short distance can be used to judge the proximity. In this paper, Wi-Fi RSSI based ranging model is described in (26):

$$P_r(d) = P_0(d_0) - 10\alpha\lg\left(\frac{d}{d_0}\right) + \varphi \tag{26}$$

where $P_r(d)$ indicates the RSSI at distance d from the source, d_0 is the reference distance, $P_0(d_0)$ is the RSSI at distance d_0, α is the path loss exponent, and φ is the Gaussian random variable with a mean of zero.

The final Wi-Fi ranging is the combination of distances calculated by the (25) and (26) which can improve the short-distance performance of Wi-Fi FTM and also maintain the long-distance accuracy.

$$\Delta D_{\text{Fused}} = \delta_1 \cdot L_{\text{observed}} + \delta_2 \cdot P_r(d) \tag{27}$$

where $\delta_1 + \delta_2 = 1$, ΔD_{Fused} indicates the fused distance between smartphone and Wi-Fi AP. $\delta_2 = -\gamma / \text{RSSI}$, because the accuracy of Wi-Fi RSSI based ranging model would decline with the measured distance, thus, threshold γ is set to adjust the weight of RSSI based ranging model, which is calculated by the standard deviation of Wi-Fi RSSI in distance of 1m.

When the pedestrian passes by a local Wi-Fi AP, the proposed Wi-Fi ranging model in (27) will provide accurate distance measurement which can be used for proximity detection, and a new Wi-Fi AP based landmark point with 3D coordinate can be successfully detected when the ranging result reaches the set threshold. The description of proximity detection is shown in Fig.4.

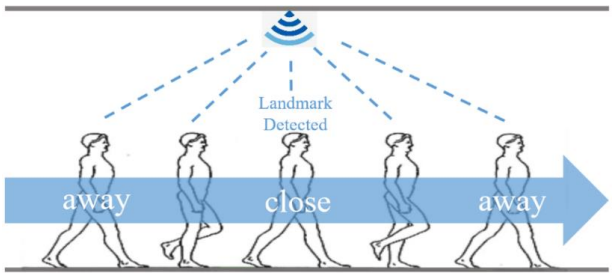

Fig. 4. Procedure of Proximity Detection

B. Integrated Localization Based on Wi-Fi FTM and Built-in Sensors

This paper provides built-in sensors based positioning method and Wi-Fi FTM ranging method to estimate pedestrian position. The two methods have their own advantages and disadvantages. Wi-Fi FTM based ranging method can provides exact coordinates directly, but is affected by NLOS. Built-in sensors estimation is more accurate within a short distance, but there is a cumulative error as distance increases. This paper combines the two methods to overcome the shortcomings of each. The estimation based on Wi-Fi FTM could eliminate the cumulative error caused by built-in sensors estimation, and built-in sensors estimation has good time-recursive performance to avoid instantaneous deviation. Therefore, this paper introduces the UPF to combine the two methods, which would improve the further localization accuracy.

In the process of fusion, the walking speed, heading information calculated by AEKF and altitude information calculated by barometer are used as state value, and fused distances and altitude provided by Wi-Fi FTM and landmark are used as the observed value. The system state equation is as follows:

$$\boldsymbol{X}(t) = \begin{bmatrix} x(t) \\ y(t) \\ z(t) \end{bmatrix} = \boldsymbol{A}\begin{bmatrix} x(t-1) \\ y(t-1) \\ z(t-1) \end{bmatrix} + \boldsymbol{B}S(t) + \boldsymbol{v} \tag{28}$$

where $\boldsymbol{X}(t) = [x(t)\ \ y(t)\ \ z(t)]^{\mathrm{T}}$ is the 3D location of the pedestrian at time t, $\boldsymbol{A}$ and $\boldsymbol{B}$ are unit matrixes, $S(t) = [V(t)\cdot\Delta\delta\cdot\sin\theta(t)\ \ V(t)\cdot\Delta\delta\cdot\cos\theta(t)\ \ \Delta\eta(t)]^{\mathrm{T}}$, $\Delta\delta$ indicates the update rate of UPF, $\Delta\eta(t)$ is the change of height

This article has been accepted for publication in a future issue of this journal, but has not been fully edited. Content may change prior to final publication. Citation information: DOI 10.1109/JIOT.2020.2999626, IEEE Internet of Things Journal

calculated by the barometer [52], $\boldsymbol{v}$ is the Gaussian noise with a noise matrix $\boldsymbol{W}$. The initial location $[x(0)\ \ y(0)]^{\mathrm{T}}$ is provided by the least squares (LS) algorithm which is defined in [53] and the initial altitude value $z(0)$ is provided by the detected landmark point.

The distance between mobile terminal and each Wi-Fi AP is provided by fused Wi-Fi ranging results, which can be used as observed value after pre-processing. In addition, each detected landmark point can be used to provide absolute altitude information $z(t)$. The observation equation is shown as follows:

$$\boldsymbol{Z}(t)=\begin{bmatrix}\sqrt{(x(t)-x_1)^2+(y(t)-y_1)^2}\\ \sqrt{(x(t)-x_2)^2+(y(t)-y_2)^2}\\ \vdots\\ \sqrt{(x(t)-x_j)^2+(y(t)-y_j)^2}\\ z(t)\end{bmatrix}+\boldsymbol{E} \tag{29}$$

where $\boldsymbol{E}$ indicates the random error of observed value with a noise matrix $\boldsymbol{\phi}$, $x(t)$ and $y(t)$ is estimated by system state equation, the Euclidean Distance between predicted position and each Wi-Fi AP is calculated as observation value, j is the number of Wi-Fi APs, x_j and y_j indicate the position of each Wi-Fi AP, $z(t)$ represents the predicted altitude value, real-time 3D localization can be achieved after fusion.

Different from the PF applied in [18], the UPF proposed in this paper uses the unscented Kalman filter (UKF) to provide the distribution reference in procedure of particle state updating and get a more reliable particle distribution. When the observed Wi-Fi FTM is affected by NLOS, the mean square error obtained by UKF calculation can effectively reflect the degree of the NLOS interference applied to the 3D location calculation and then adjust the particle distribution to improve the particle estimation accuracy in PF algorithm. Thus, the UPF can effectively reduce the NLOS error and combine the advantages of Wi-Fi FTM based method and multiple sensors based method to reach the high precision of localization. The whole procedure of proposed UPF is shown as follows:

1) Initialization, k=0, For i=1:N, extract the initial state from the prior distribution:

$$\begin{aligned}&X_0^{(i)}=E[X_0^{(i)}]\\ &P_0^{(i)}=E[(X_0^{(i)}-\overline{X}_0^{(i)})(X_0^{(i)}-\overline{X}_0^{(i)})^{\mathrm{T}}]\\ &\overline{X}_0^{(i)a}=E[\overline{X}_0^{(i)a}]=[(\overline{X}_0^{(i)})^{\mathrm{T}}\ 0\quad 0]^{\mathrm{T}}\\ &P_0^{(i)a}=E[(X_0^{(i)a}-\overline{X}_0^{(i)a})(X_0^{(i)a}-\overline{X}_0^{(i)a})^{\mathrm{T}}]\end{aligned} \tag{30}$$

2) Importance sampling. For i=1:N, calculate the mean and variance of state quantities using the UKF algorithm:

① Calculate Sigma point set:

$$X_{k-1}^{(i)a}=[\overline{X}_{k-1}^{(i)a}\quad \overline{X}_{k-1}^{(i)a}\pm\sqrt{(n_a+\lambda)P_{k-1}^{(i)a}}] \tag{31}$$

② Further prediction of Sigma point sets:

$$\begin{aligned}&\overline{X}_{k|k-1}^{(i)a}=f(X_{k-1}^{(i)x},X_{k-1}^{(i)v})\\ &\overline{X}_{k-1}^{(i)}=\sum_{j=0}^{2n_a}W_j^{(m)}X_{j,k|k-1}^{(i)x}\\ &P_{k|k-1}^{(i)}=\sum_{j=0}^{2n_a}W_j^{(c)}[X_{j,k|k-1}^{(i)x}-\overline{X}_{k|k-1}^{(i)}][X_{j,k|k-1}^{(i)x}-\overline{X}_{k|k-1}^{(i)}]^{\mathrm{T}}\\ &Z_{k|k-1}^{(i)}=h(X_{k|k-1}^{(i)x},X_{k-1}^{(i)n})\\ &\overline{Z}_{k|k-1}^{(i)}=\sum_{j=0}^{2n_a}W_j^{(c)}Z_{j,k|k-1}^{(i)}\end{aligned} \tag{32}$$

③ Integrate with the latest observations and update:

$$\begin{aligned}&P_{\tilde{z}_k,\tilde{z}_k}=\sum_{j=0}^{2n_a}W_j^{(c)}[Z_{j,k|k-1}^{(i)}-Z_{k|k-1}^{(i)}][Z_{j,k|k-1}^{(i)}-Z_{k|k-1}^{(i)}]^{\mathrm{T}}\\ &P_{X_k,Z_k}=\sum_{j=0}^{2n_a}W_j^{(c)}[X_{j,k|k-1}^{(i)}-\bar{X}_{k|k-1}^{(i)}][X_{j,k|k-1}^{(i)}-\bar{X}_{k|k-1}^{(i)}]^{\mathrm{T}}\\ &K_k=P_{\tilde{z}_k,\tilde{z}_k}P_{X_k,Z_k}\\ &\bar{X}_k^{(i)}=\bar{X}_{k|k-1}^{(i)}+K_k(Z_k-\bar{Z}_{k|k-1}^{(i)})\\ &\hat{P}_k^{(i)}=P_{k|k-1}^{(i)}-K_kP_{\tilde{z}_k,\tilde{z}_k}K_k^{\mathrm{T}}\end{aligned} \tag{33}$$

④ Calculate samples and update particles:

$$\begin{aligned}&\hat{X}_k^{(i)}\sim q(X_k^{(i)}\mid X_{0:k-1}^{(i)},Z_{1:k})=N(\bar{X}_k^{(i)},\hat{P}_k^{(i)})\\ &\hat{X}_{0:k}^{(i)}\sim(X_{0:k-1}^{(i)},\hat{X}_k^{(i)})\\ &\hat{P}_{0:k}^{(i)}\sim(P_{0:k-1}^{(i)},\hat{P}_k^{(i)})\end{aligned} \tag{34}$$

For i=1:N, recalculate weights for each particle:

$$w_k^{(i)}=\frac{p(Z_k\mid\hat{X}_k^{(i)})p(\hat{X}_k^{(i)}\mid X_k^{(i)})}{q(\hat{X}_k^{(i)}\mid X_{0:k}^{(i)},Z_{1:k})} \tag{35}$$

For i=1:N, normalize weight:

$$\tilde{w}_k(X_{0:k}^{(i)})=\frac{w_k(X_{0:k}^{(i)})}{\sum_{i=1}^{N}w_k(X_{0:k}^{(i)})} \tag{36}$$

3) Re-sampling: Using the re-sampling algorithm to copy and eliminate the particle set $X_{0:k}^{(i)}$ according to the normalized weight:

$$w_k^i=\tilde{w}_k^i=\frac{1}{N} \tag{37}$$

4) Output final filtering result:

$$X_k^{(i)}=\frac{1}{N}\sum_{i=1}^{N}w_{0:k}^iX_{0:k} \tag{38}$$

In the procedure of proposed UPF based localization, the complexity of UKF depends on the dimension of system state value in Equation (28), which is constant in this work. Thus, the final complexity of UPF depends on the number of selected particles, we will give the relationship evaluation between complexity and localization accuracy and provide the optical results in Section V.

V. Experimental Results of 3D-WFBS

In this section, a series of experiments are designed to verify

This article has been accepted for publication in a future issue of this journal, but has not been fully edited. Content may change prior to final publication. Citation information: DOI 10.1109/JIOT.2020.2999626, IEEE Internet of Things Journal

the accuracy of proposed AEKF and final 3D-WFBS, two typical indoor scenes are selected as experimental sites. In this work, Wi-Fi APs use Intel 8260 Wireless cards and Ubuntu 16.04 LTS as hardware and software platforms, Google Pixel 3 is used as mobile terminal which supports Android 9 based Wi-Fi FTM and can get real-time RTT and RSSI data from surrounding Wi-Fi APs. In addition, the Google Pixel 3 contained rich sensors needed by PDR such as the accelerometer, gyroscope, magnetometer and barometer. The sampling rates of built-in sensors and Wi-Fi FTM was 100 Hz and 4 Hz respectively. The real-time location information calculated by UPF was acquired with frequency of 4 Hz. Timestamps within the multi-sensor method and Wi-Fi FTM were synchronized based on the time when RTT data is updated.

A. Accuracy Estimation of AEKF

The AEKF algorithm proposed in this paper combines characteristics of different kinds of built-in sensors to overcome their disadvantages respectively. In this paper, only the handheld mode of smartphone is considered, which is described in [38]. The experiment in this work selects a 2D rectangular corridor as the experimental site to estimate the accuracy of AEKF based heading and walking speed fusion, which is shown in Fig.5(a). The selected experimental site contains magnetic interference which may cause measured error in magnetometer data, as shown in Fig.5(b):

Fig. 5(a). Experimental Site and Reference Track

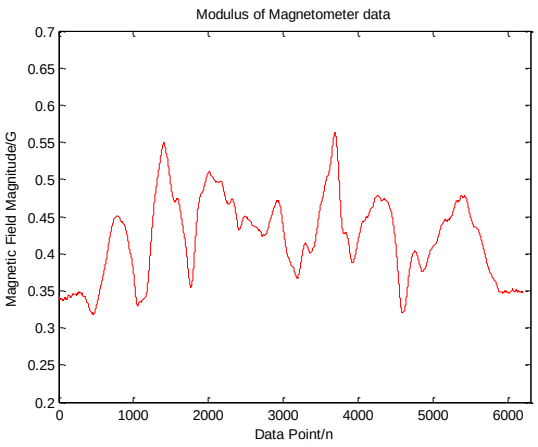

Fig. 5(b). Distribution of Magnetic Field

In order to evaluate the long-time accuracy between gyroscope update and the proposed AEKF, testers conducted a continuous walking test, pedestrians started from the reference point A, passed through point B, C, and D, then returned to point A, and turned to the original orientation. The reference headings are 115˚, 205˚, 295˚, and 25˚ between each two reference points. This procedure repeated 11 times on the same route continuously, the heading comparison results are shown in Fig.6:

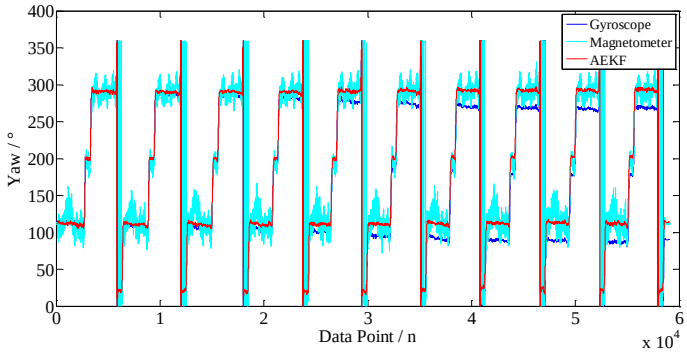

Fig.6. Heading Comparison of Long-time Walking

The Fig.6 shows that the cumulative error exists in the heading calculated by the gyroscope and increases with time, the output heading of gyroscope cannot reflect the true heading after a period time of use. The heading angle output by the magnetometer is subject to large fluctuations due to magnetic interference and cannot reflect the true heading angle. However, due to the real-time adjustment of the observed noise covariance matrix for the magnetic interference in the proposed AEKF, in the case of presence of magnetic interference, the system can focus on the gyroscope based calculation to reduce the external magnetic interference to the heading, and when the QSMF period is detected, the gyroscope drift error can be corrected by increasing the weight of the magnetometer, thus the fused heading angle is closer to the reference heading. In Fig. 6, the pedestrian's heading calculated by gyroscope drifts about 30˚after walking for around 20 minutes, while the fused heading remain stable and high accuracy, drifts only about 4˚.

In order to evaluate the accuracy of proposed speed fusion algorithm in AEKF, 10 testers are required to walk straight forward in a corridor for 50 m and then calculate the deviation between calculated distance and ground-truth distance, the test results using three kinds of speed calculation methods proposed above are shown in Fig.7:

This article has been accepted for publication in a future issue of this journal, but has not been fully edited. Content may change prior to final publication. Citation information: DOI 10.1109/JIOT.2020.2999626, IEEE Internet of Things Journal

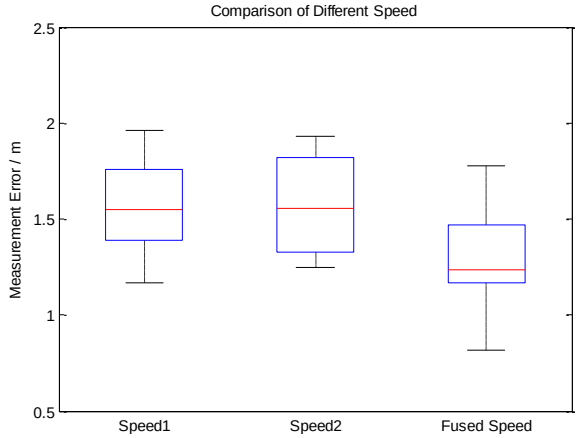

Fig.7. Comparison of Different Walking Speed

It can be seen from the Fig.7 that the two kinds of walking speed estimation algorithm prove the similar performance of distance measurement, while the fused speed by AEKF effectively improves the estimation accuracy.

B. Accuracy Evaluation of Ranging Fusion and Proximity Detection

Different types of noise interference occur when using Wi-Fi FTM and RSSI for distance measurement between mobile terminal and smartphone. For instance, Wi-Fi FTM is affected by NLOS and random error, while RSSI is objected to multipath propagation and is more accurate for short-distance measurement. Thus, the proposed distance fusion model combines the two different kinds of ranging methods and overcome the shortcomings of each. The final ranging accuracy is shown in Fig.8:

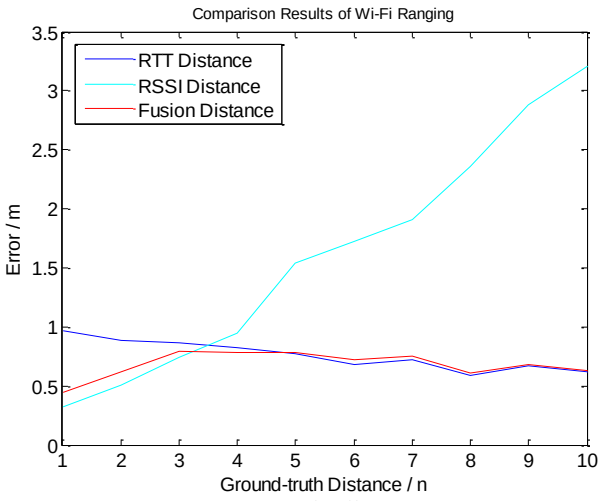

Fig.8. Accuracy Comparison of Different Ranging Methods

Fig.8 compares the CDF errors at 67.5% between three different Wi-Fi ranging methods, the results show that RSSI based ranging method proves decreasing accuracy with distance while the fusion method maintains high accuracy. Thus, the fused distance is used to recognize the landmark point when the pedestrian passes a local Wi-Fi AP, the detection result is shown in Fig.9:

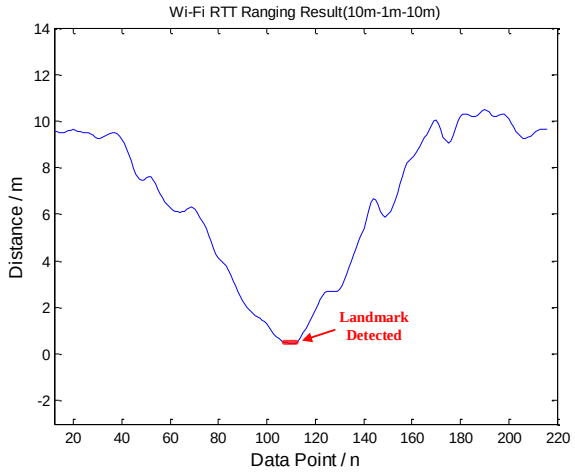

Fig.9. Landmark Detection Result by Fused Distance

The landmark point recognition error can be acquired by calculating the Euclidean distance between the real coordinates and the identified coordinates. Fig.10 demonstrates that the Wi-Fi AP based landmark detection errors ranges from 0.25 m to 0.64 m and the median error is about 0.4 m. The detected landmark points are further used to provide absolute reference to barometer based altitude calculation.

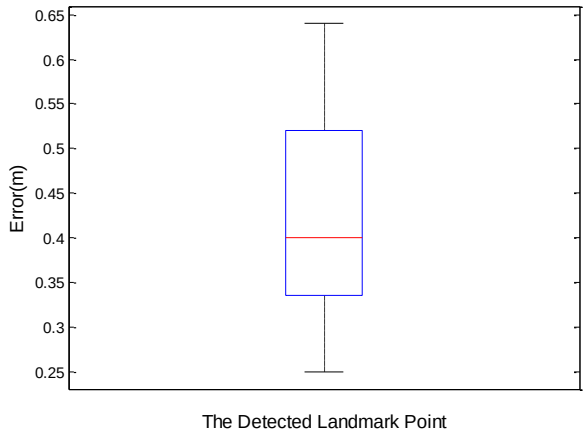

Fig.10. Landmark Detection Error of Wi-Fi AP

C. Accuracy Evaluation of 3D-WFBS

Section *A* presents the accuracy of the AEKF-based heading and walking speed fusion and section *B* evaluates the performance of Wi-Fi ranging and proximity detection. In order to estimate the localization accuracy of proposed 3D-LWBS, two adjacent floors in a 3D building are selected as the experimental site, Fig.11 shows the maps of two floors and the deployment of Wi-Fi APs. The distribution of Wi-Fi APs follows the optimal geometric distribution to reduce the number of required APs, each room contains 4 APs in the different corners and the corridor or stairwell contains 3 APs. The testers started from position A, walked pass the position B, C, D, E, F, G, H, I, J, K, L, and finally return back to the position A, going up and down stairs are contained in the walking route. The walking path is shown in Fig.11(a) and Fig.11(b).

This article has been accepted for publication in a future issue of this journal, but has not been fully edited. Content may change prior to final publication. Citation information: DOI 10.1109/JIOT.2020.2999626, IEEE Internet of Things Journal

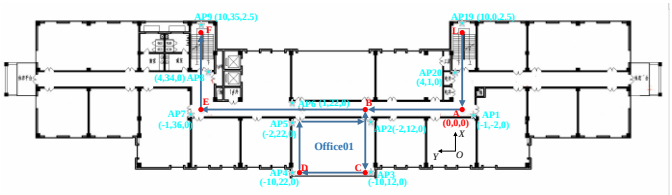

Fig.11(a). Walking Route at the 4th Floor

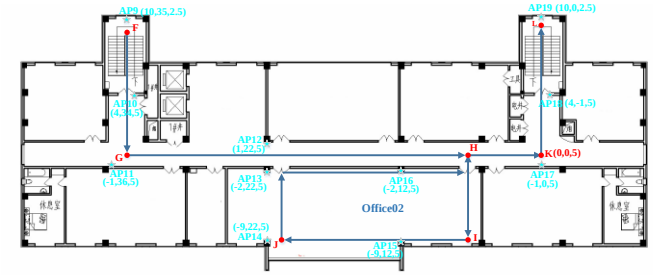

Fig.11(b). Walking Route at the 5th Floor

The comparison results of AEKF based PDR and proposed 3D-LWBS are shown in Fig.12:

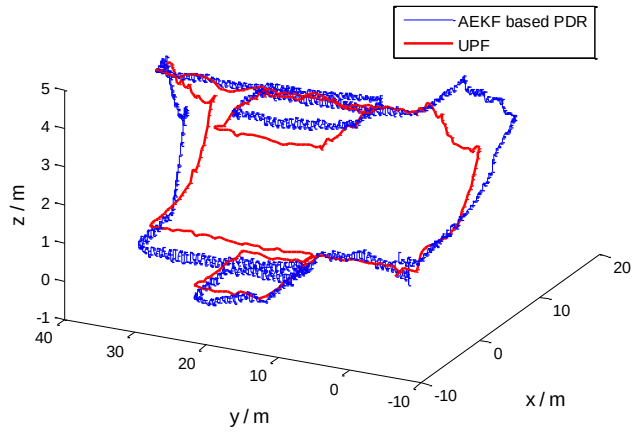

Fig.12. Comparison of AEKF based PDR and 3D-LWBS

It can be seen from Fig.12 that AEKF based PDR method proves high accuracy in a short time, but the positioning error increases when the pedestrian goes up or down stairs. After fusion, the positioning accuracy remain stable whether in the cases of going upstairs or walking on the same floor.

This process was continuously repeated 10 times in order to estimate the long-term accuracy of 3D-WFBS compared with AEKF based PDR algorithm. The 2D positioning error was estimated by calculating the Euclidean distance between pedestrian's real-time position and location of reference points B, D, H, and J. The comparison results of 2D positioning errors

TABLE II
ACCURACY COMPARISON BETWEEN DIFFERENT SCENES

Algorithm \ Scene	Office Accuracy /m	Corridor Accuracy /m	Staircase Accuracy /m	Calculation Time /ms
UKF	1.82	1.76	1.91	1.15
PF	1.56	1.42	1.38	3.62
UPF	1.02	1.12	1.15	4.72

at each reference point are shown in Fig.13:

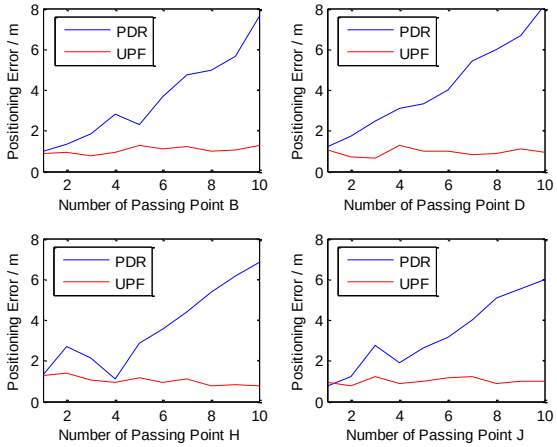

Fig.13. Comparison of 2D Positioning Error

The altitude error was estimated by calculating deviation between pedestrian's real-time altitude and altitude information of reference points A, F, G, L. The comparison results of altitude errors at each reference point are shown in Fig.14:

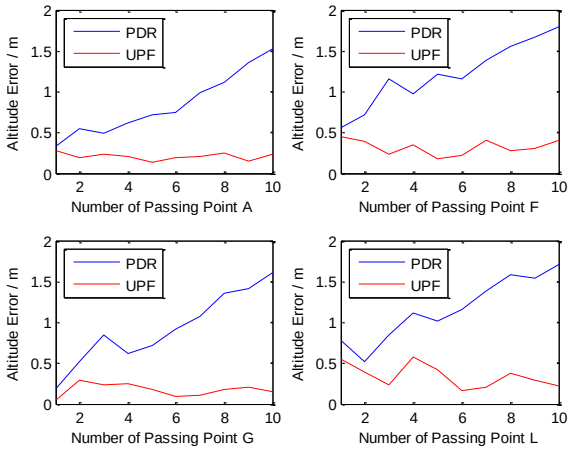

Fig.14. Comparison of Altitude Error

It can be seen from Fig.13 and Fig.14 that AEKF based PDR is still subjected to cumulative error and the 2D positioning accuracy increases with time which can reach 8m or higher and the altitude information calculated by barometer also cumulates with time because the altitude estimation in PDR is also achieved by calculating the deviation of altitude between adjacent timestamps. The comparison of CDF errors between PDR and proposed 3D-WFBS is shown in Fig.15:

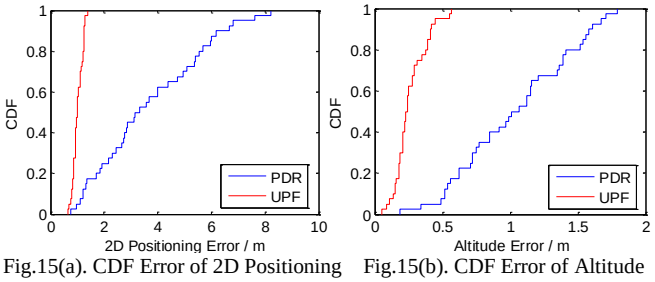

Fig.15(a). CDF Error of 2D Positioning Fig.15(b). CDF Error of Altitude

This article has been accepted for publication in a future issue of this journal, but has not been fully edited. Content may change prior to final publication. Citation information: DOI 10.1109/JIOT.2020.2999626, IEEE Internet of Things Journal

It can be found from Fig.15 that the proposed 3D-WFBS maintains high accuracy and gets the final CDF error within 1.11 m at 67.5% after a long-time use. The altitude accuracy also shows the high level and the CDF error is within 0.28 m at 67.5%.

In order to estimate the accuracy of proposed UPF and other kinds of fusion methods, UKF and PF are selected as contrast algorithms. The number of particles in UPF and PF are the same as 100, point E and point F are chose as reference points to evaluate the 2D and altitude accuracy, comparison results are shown in Fig.16:

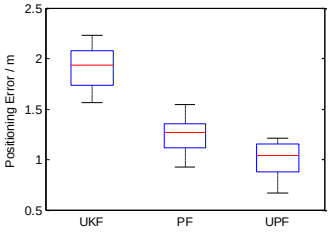

Fig.16(a). 2D Positioning Error at Point E

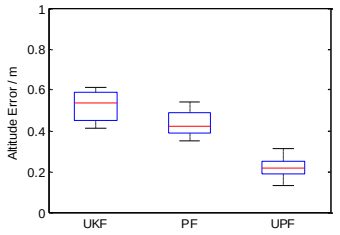

Fig.16(b). Altitude Error at Point F

It can be seen from Fig.16 that compared with UKF, Monte Carlo based PF effectively improve the 3D positioning accuracy, while the proposed UPF combines the advantages of UKF and PF and further improves the positioning accuracy.

Finally, we give a comprehensive comparison between proposed UPF and the previous UKF and PF, which are proposed in references [17] and [18]. We divide the indoor scenes into three kinds: the office which contains the test points D and J, the corridor which contains the test points B and H, and the staircase which contains the test points F and L, then calculate the CDF errors of different positioning methods in 67.5% in corresponding scenes. The calculation time is defined as the difference of smartphone based timestamps during one UPF period, which depends on the computational ability of the smartphone. The localization errors in different scenes and the required calculation time in case of 100 particles are shown in Table II. The accuracy comparison between PF and UPF in case of different number of particles is shown in Fig.17.

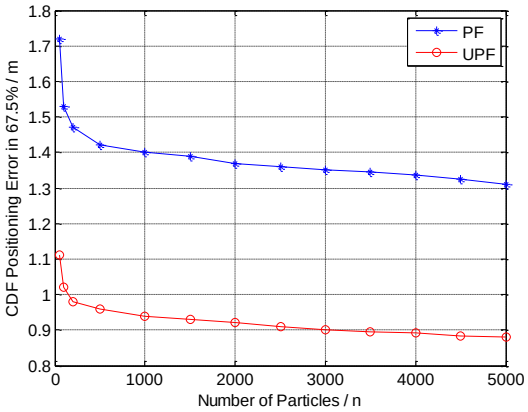

Fig.17. Accuracy Comparison Using Different Number of Particles

It can be found in Table II and Fig.17 that the proposed UPF based 3D-WFBS proves better localization performance in different indoor environments such as office, corridor and staircase while the calculation delay makes little effect in the procedure of real-time localization. In addition, the localization accuracy proves better improvement when the number of particles increases from 50 to 100 compared with more particles. The high precision positioning results can widely be applied in the fields of IoT and AI.

VI. Conclusion

In order to improve the accuracy and stability of indoor localization, this paper proposes 3D-WFBS algorithm, which is divided into three parts: (1) AEKF based PDR: using collected built-in sensors data to provide accurate and stable heading and walking speed information; (2) Combining RTT and RSSI to estimate the distance between the Wi-Fi APs and pedestrian with smartphone, and using fused distance to detect Wi-Fi AP based landmark in order to provide absolute altitude reference; (3) Integrated localization using UPF. The combination of Wi-Fi FTM based method and built-in sensor based method effectively improve the positioning accuracy and stability. The final CDF error of 2D positioning is within 1.11 m at 67.5% and the altitude error is within 0.28 m at 67.5%.

This paper is closed with a brief discussion of the future works. In the future, it is foreseen that the precise positioning results provided by Wi-Fi FTM and multiple sensors can gain further improvement because more and more Wi-Fi chipsets in mobile devices supporting large bandwidth transmission. Besides, other observations extracted from Wi-Fi APs such as angle of arrival (AOA), channel state information (CSI) which can provide accurate measured angle information, the smartphone based single Wi-Fi station positioning would become possible in the future.

References

[1] P. Davidson and R. Piché, “A survey of selected indoor positioning methods for smartphones,” IEEE Communications Surveys & Tutorials, vol.19, no.2, pp.1347-1370, 2016.

[2] Y. Li, Y. Zhuang, P. Zhang, et al., “An improved inertial/wifi/magnetic fusion structure for indoor navigation,” Information Fusion, vol.34, pp.101-119, July. 2017.

[3] M. R. Mahfouz, C. Zhang, B. C. Merkl, et al., “Investigation of high-accuracy indoor 3-D positioning using UWB technology,” IEEE Transactions on Microwave Theory and Techniques, vol.56, no.6, pp.1316-1330, June. 2008.

[4] N. Yu, X. Zhan, S. Zhao, et al., “A precise dead reckoning algorithm based on bluetooth and multiple sensors,” IEEE Internet of Things Journal, vol.5, no.1, pp.336-351, Feb. 2018.

[5] B. Jang and H. Kim, “Indoor positioning technologies without offline fingerprinting map: A survey,” IEEE Communications Surveys & Tutorials, vol.21, no.1, pp.508-525, FIRST QUARTER. 2018.

[6] R.Z. Chen, W. Chen, X. Chen, et al., “Sensing strides using EMG signal for pedestrian navigation,” GPS solutions, vol.15, no.2, pp.161-170, 2011.

[7] S. Beauregard and M. Klepal, “Indoor PDR performance enhancement using minimal map information and particle filters,” in IEEE Location and Navigation Symposium, 2008, pp.141-147.

[8] B. Zhou, Q. Li, Q. Mao, et al., “Activity sequence-based indoor pedestrian localization using smartphones,” IEEE Transactions on Human-Machine Systems, vol.45, no.5, pp.562-574, 2014.

[9] J. Shang, X. Hu, W. Cheng, et al., “Gridiloc: A backtracking grid filter for fusing the grid model with PDR using smartphone sensors,” Sensors, vol.16, no.12, pp.2137-2159, 2016.

[10] H. Liu, H. Darabi, P. Banerjee, et al., "Survey of wireless indoor positioning techniques and systems," IEEE Transactions on Systems, Man, and Cybernetics, vol.37, no.6, pp.1067-1080, Nov. 2007.

[11] S. He and S. –H. G. Chan, "Wi-Fi fingerprint-based indoor positioning: Recent advances and comparisons," IEEE Communications Surveys & Tutorials, vol.18, no.1, pp.466-490, FIRST QUARTER. 2015.

[12] L. Chen, K. Yang and X. Wang, "Robust cooperative Wi-Fi fingerprint-based indoor localization," IEEE Internet of Things Journal, vol.3, no.6, pp.1406-1417, Dec. 2016.

[13] Y. Li, Z. He, Z. Gao, et al., "Toward Robust Crowdsourcing-Based Localization: A Fingerprinting Accuracy Indicator Enhanced Wireless/Magnetic/Inertial Integration Approach," IEEE Internet of Things Journal, vol.6, no.2, pp.3585-3600, 2018.

[14] Y. Zhuang, J. Yang, L. Qi, et al., "A pervasive integration platform of low-cost MEMS sensors and wireless signals for indoor localization," IEEE Internet of Things Journal, vol.5, no.6, pp.4616-4631, Dec. 2017.

[15] IEEE Computer Society LAN/MAN Standards Committee. IEEE Standard for Information technology-Telecommunications and information exchange between systems-Local and metropolitan area networks-Specific requirements Part 11: Wireless LAN Medium Access Control (MAC) and Physical Layer (PHY) Specifications. IEEE Std 802.11, 2016.

[16] M. Ibrahim, H. Liu, M. Jawahar, et al., "Verification: Accuracy evaluation of WiFi fine time measurements on an open platform," in Proceedings of the 24th Annual International Conference on Mobile Computing and Networking. ACM, 2018, pp.417-427.

[17] Y. Yu, R. Chen, L. Chen, et al., "A Robust Dead Reckoning Algorithm Based on Wi-Fi FTM and Multiple Sensors," Remote Sensing, vol.11, no.5, pp.504-526, Mar. 2019.

[18] S. Xu, R. Chen, Y. Yu, et al., "Locating Smartphones Indoors Using Built-In Sensors and Wi-Fi Ranging With an Enhanced Particle Filter," IEEE Access, vol.7, pp.95140-95153, Aug. 2019.

[19] D. Ciuonzo and P. Salvo Rossi, "Quantizer design for generalized locally optimum detectors in wireless sensor networks." IEEE Wireless Communications Letters, vol.7, no.2, pp.162-165, 2017.

[20] Arian Shoari and Alireza Seyedi, "On localization of a non-cooperative target with non-coherent binary detectors." IEEE Signal Processing Letters, vol.21, no.6, pp.746-750, 2014.

[21] D. Ciuonzo and P. Salvo Rossi, "Distributed detection of a non-cooperative target via generalized locally-optimum approaches." Information Fusion vol.36, pp.261-274, 2017.

[22] F. Tlili, A. Rachedi, A. Benslimane, "Time-bounded localization algorithm based on distributed multidimensional scaling for wireless sensor networks," 2014 IEEE International Conference on Communications (ICC), IEEE, pp. 233-238, 2014.

[23] F. Khelifi, A. Bradai, S. Amri, A. Rachedi, M. L. Kaddachi, "A new fuzzy logic based node localization mechanism for Wireless Sensor Networks" Future Generation Computer Systems, vol.93, pp.799-813, 2019.

[24] S. Hamdoun A. Rachedi, A. Benslimane, "Comparative analysis of RSSI-based indoor localization when using multiple antennas in Wireless Sensor Networks," 2013 International Conference on Selected topics in mobile and wireless networking (MoWNeT), IEEE, pp.146-151, Aug.2013.

[25] S. Hamdoun, A. Rachedi, A. Benslimane, "RSSI-based Localization Algorithms using Spatial Diversity in Wireless Sensor Networks," International Journal of Ad Hoc and Ubiquitous Computing, Inderscience, vol.19, pp.157-167, 2015.

[26] X. Wang, L. Gao, S. Mao, "CSI phase fingerprinting for indoor localization with a deep learning approach," IEEE Internet of Things Journal, vol.3, pp.1113-1123, 2016.

[27] Z. He, Y. Ma and R. Tafazolli, "Improved high resolution TOA estimation for OFDM-WLAN based indoor ranging," IEEE Wireless Communications Letters, vol.2, no.2, pp.163-166, 2013.

[28] M. Rea, A. Fakhreddine, D. Giustiniano, et al., "Filtering noisy 802.11 time-of-flight ranging measurements from commoditized wifi radios," IEEE/ACM Transactions on Networking, vol.25, no.4, pp.2514-2527, 2017.

[29] L. Banin, U. Schatzberg and Y. Amizur, "Next generation indoor positioning system based on WiFi time of flight," in Proc. 26th Int. Tech. Meeting Satellite Division Inst. Navigat, 2013, pp.975-982.

[30] U. Schatzberg, L. Banin and Y. Amizur, "Enhanced WiFi ToF indoor positioning system with MEMS-based INS and pedometric information," in 2014 IEEE/ION Position, Location and Navigation Symposium-PLANS. IEEE, 2014, pp.185-192.

[31] N. Dvorecki, O. Bar-Shalom, L. Banin L, et al., "A Machine Learning Approach for Wi-Fi RTT Ranging," in 2019 IEEE/ION Position, IEEE, 2019, pp.118-123.

[32] U. Niesen, V. N. Ekambaram, J. Jose, et al., "Intervehicle Range Estimation From Periodic Broadcasts," IEEE Transactions on Vehicular Technology, vol.66, no.12, PP.10637-10646, 2017.

[33] L. Banin, U. Schatzberg and Y. Amizur, "Wifi ftm and map information fusion for accurate positioning," in 2016 International Conference on Indoor Positioning and Indoor Navigation (IPIN). Oct. 2016, pp.4-7.

[34] R. Harle, "A survey of indoor inertial positioning systems for pedestrians," IEEE Communications Surveys & Tutorials, vol.15, no.3, pp.1281-1293, THIRD QUARTER 2013.

[35] L. E. Díez, A. Bahillo, J. Otegui, et al., "Step length estimation methods based on inertial sensors: a review," IEEE Sensors Journal, vol.18, no.17, pp.6908-6926, Sept. 2018.

[36] A. Martinelli, H. Gao, P. D. Groves, et al., "Probabilistic context-aware step length estimation for pedestrian dead reckoning," IEEE Sensors Journal, vol.18, no.4, pp.1600-1611, Feb. 2017.

[37] E. Foxlin, "Pedestrian tracking with shoe-mounted inertial sensors," IEEE Computer graphics and applications, vol.5, pp.38-46, Dec. 2005.

[38] X. Tong, Y. Su, Z. Li, et al., "A Double-step Unscented Kalman Filter and HMM-based Zero Velocity Update for Pedestrian Dead Reckoning Using MEMS Sensors," IEEE Transactions on Industrial Electronics, vol.67, no.1, pp.581-591, Jan. 2019.

[39] V. Renaudin, C. Combettes and F. Peyret, "Quaternion based heading estimation with handheld MEMS in indoor environments," in 2014 IEEE/ION Position, Location and Navigation Symposium-PLANS. IEEE, 2014, pp.645-656.

[40] H. Weinberg, "Using the ADXL202 in pedometer and personal navigation applications," Analog Devices AN-602 application note, vol.2, no.2 pp.1-6, 2002.

[41] J. Kuang, X. Niu and X. Chen, "robust pedestrian dead reckoning based on MEMS-IMU for smartphones," Sensors, vol.18, no.5, pp.1391-1409, 2018.

[42] L. Fang, P. J. Antsaklis, L. A. Montestruque, et al., "Design of a wireless assisted pedestrian dead reckoning system-the NavMote experience," IEEE transactions on Instrumentation and Measurement, vol.54, no.6, pp.2342-2358, Dec. 2005.

[43] C. Combettes and V. Renaudin, "Walking direction estimation based on statistical modeling of human gait features with handheld MIMU," IEEE/ASME Transactions on Mechatronics, vol.22, no.6, pp.2502-2511, Dec.2017.

[44] A. Zanella, "Best practice in RSS measurements and ranging," IEEE Communications Surveys & Tutorials, vol.18, no.4, pp.2662-2686, THIRD QUARTER. 2016.

[45] I. Sharp and K. Yu, "Indoor TOA error measurement, modeling, and analysis," IEEE Transactions on Instrumentation and Measurement, vol.63, no.9, pp.2129-2144, Sept. 2014.

[46] Y. T. Chan, W. Y. Tsui, H. C. So, et al., "Time-of-arrival based localization under NLOS conditions," IEEE Transactions on Vehicular Technology, vol.55, no.1, pp.17-24, Jan. 2006.

[47] J. Qian, J. Ma, R. Ying, et al., "An improved indoor localization method using smartphone inertial sensors," in International Conference on Indoor Positioning and Indoor Navigation. IEEE, 2013, pp.1-7.

[48] J. Jahn, U. Batzer, J. Seitz, et al., "Comparison and evaluation of acceleration based step length estimators for handheld devices," in 2010 International Conference on Indoor Positioning and Indoor Navigation. IEEE, 2010, pp.1-6.

[49] R. Chen, L. Pei L and Y. Chen, "A smart phone based PDR solution for indoor navigation," in Proceedings of the 24th international technical meeting of the satellite division of the institute of navigation, 2011, pp.1404-1408.

[50] M. Ma, Q. Song, Y. Li, et al., "A heading error estimation approach based on improved Quasi-static magnetic Field detection," in 2016 International Conference on Indoor Positioning and Indoor Navigation (IPIN). IEEE, 2016, pp.1-8.

[51] W. Xue, W. Qiu, X. Hua, et al., "Improved Wi-Fi RSSI measurement for indoor localization," IEEE Sensors Journal, vol.17, no.7, pp.2224-2230, Apr. 2017.

[52] Y. Li, Z. Gao, Z. He, et al., "Multi-sensor multi-floor 3D localization with robust floor detection," IEEE Access, vol.6, pp.76689-76699, Nov. 2018.

[53] H. Liu, H. Darabi, P. Banerjee, et al., "Survey of wireless indoor positioning techniques and systems," IEEE Transactions on Systems, Man, and Cybernetics, vol.37, no.6, pp.1067-1080, Nov. 2007.

This article has been accepted for publication in a future issue of this journal, but has not been fully edited. Content may change prior to final publication. Citation information: DOI 10.1109/JIOT.2020.2999626, IEEE Internet of Things Journal

Yue Yu received the B.S. and M.S. degrees from the Chongqing University of Posts and Telecommunications. He is currently pursuing the Ph.D. degree in geodesy and survey engineering from Wuhan University, Wuhan, Hubei, China. His research interests include the inertial positioning and navigation technology, indoor positioning and navigation technology based on chance signal, signal processing and fusion technology.

Ruizhi Chen is currently a Professor and the Director of the State Key Laboratory of Information Engineering in surveying, mapping, and remote sensing with Wuhan University. He was an Endowed Chair Professor with Texas A&M University Corpus Christi, USA, the Head and a Professor of the Department of Navigation and Positioning, Finnish Geodetic Institute, Finland, and the Engineering Manager of Nokia, Finland. He has published two books and more than 200 scientific papers. His current research interests include indoor positioning, satellite navigation, and location-based services.

Liang Chen is currently a professor of State Key Laboratory of Surveying, Mapping and Remote Sensing Information Engineering, Wuhan University. He was a senior researcher in Finnish Geodesy Institute, deputy head of Sensors and Indoor Navigation Research Group, research leader in Finnish Laser Radar National Excellent Innovation Center. His research interests include navigation based on new signal theory and method, smartphone ubiquitous positioning and indoor and outdoor seamless localization and navigation.

Shihao Xu received the B.S. degree in Surveying and Mapping Engineering from China University of Mining and Technology, Jiangsu, China in 2019, and he is pursuing the M.S. degree in Geodesy and Survey Engineering from Wuhan University, Wuhan, Hubei, China. His research interests include the development of location-based services, indoor positioning and navigation technology, and information fusion.

Wei Li received his both B.S and M.S degrees in Surveyingand Mapping from Beijing University of Civil Engineering and Architecture. Currently he is pursuing his D.S.degree in Geodesy and Survey Engineering from Wuhan University Wuhan, Hubei, China. His research interests include indoor positioning and navigation, and sensor fusion.

Yuan Wu received the B. S. degree in computer science and technology from Southwest University, China in 2016. He got his M.S. degree in computer application technology from Institute of Automation, Chinese Academy of Sciences, China in 2019. He is currently pursuing the Ph.D. degree in Geodesy and Survey Engineering from State Key Laboratory of Information Engineering in Surveying, Mappping and Remote Sensing, WuHan University, WuHan, HuBei, China. His research interests include indoor positioning and navigation, information fusion, and location-based services.

Haitao Zhou received the M.S. degree in Geodesy and surveying engineering from Information Engineering University, Zhengzhou, China in 2016, and he is pursuing the Ph.D. degree in Geodesy and Surveying Engineering from Wuhan University, Hubei, China. His research interests include surveying data processing and GNSS precise positioning.